



Microstructure and indentation mechanical properties of YSZ nanostructured coatings obtained by suspension plasma spraying

P. Carpio ^a, E. Rayón ^b, L. Pawłowski ^c, A. Cattini ^{c,d}, R. Benavente ^b, E. Bannier ^{a,*},
M.D. Salvador ^b, E. Sánchez ^a

^a Instituto de Tecnología Cerámica (ITC). Universitat Jaume I. Castellón, Spain

^b Instituto de Tecnología de Materiales (ITM). Universidad Politécnica de Valencia. Valencia, Spain

^c Science des Procédés Céramiques et de Traitements de Surface (SPCTS, UMR CNRS 7315). Université de Limoges. Limoges, France

^d Dipartimento di Ingegneria dei Materiali e dell'Ambiente. Università degli Studi di Modena e Reggio Emilia. Modena, Italy

ARTICLE INFO

Available online 4 October 2012

Keywords:

Suspension plasma spraying
Yttria stabilised zirconia
Thermal barrier coating
Indentation

ABSTRACT

A commercial nanosuspension of yttria-stabilised zirconia (YSZ) was successfully deposited on austenitic stainless steel substrate by suspension plasma spraying technique (SPS). A SG-100 torch with internal radial injection was used for the spraying. The pneumatic system transported the feed suspension from the containers to the plasma torch. In order to study the effect of the spraying parameters, a factorial model was used to design the experiments, changing both spraying translation speed and suspension flow rate. The coating microstructure was characterised by FEG-SEM. All coatings displayed a *two-zone* microstructure formed by nanometre-sized particles surrounded by fully molten areas. Moreover, crystalline phases were determined by XRD and Raman spectroscopy. Mechanical properties were also determined using nanoindentation technique. Nanoindentation tests showed a bimodal distribution of the mechanical properties (hardness and Young's modulus) which is related to the two zones (molten and partially molten) present in the coatings.

© 2012 Elsevier B.V. All rights reserved.

1. Introduction

Nanostructured coatings have been extensively studied in the last decade and thermal spraying is one of the techniques commonly used to obtain such layers. In fact, coatings which exhibit different architectures and interesting properties can be obtained by using nanostructured feedstock in plasma spraying. In the case of YSZ coatings for thermal barriers, nanostructured coatings can offer better performance than that of their conventional counterparts as reported elsewhere [1,2]. In particular, literature shows that the non-molten nanostructured zones present in YSZ coatings obtained by atmospheric plasma spraying (APS) decrease the thermal conductivity and increase the thermal shock resistance of the thermal barriers [3]. However, nanoparticles cannot be injected directly in the plasma plume, due to their low weight and poor flowability [4]. One possible solution is to use a carrier liquid and to inject a suspension of nanoparticles inside the plasma plume instead of a powder. This process is known as suspension plasma spraying (SPS) [5,6].

Previous research has shown that thermal barrier coatings (TBCs) obtained by SPS exhibit lower thermal conductivity and higher thermal shock resistance without substantially varying the hardness or elastic modulus due to higher segmentation crack densities [7,8,10]. However, the deposition rate of SPS technique is much smaller than that of

conventional APS technique. This makes it difficult to obtain thick coatings. Thickness of SPS coatings ranges typically from 30 to 70 µm. Nevertheless, TBCs obtained by SPS usually display a lower thermal conductivity than that of other kinds of TBCs allowing coatings with lower thickness and similar thermal resistance [8,9].

As a consequence of the low thickness of the SPS coatings, it was found that nanoindentation technique is a more feasible method than conventional microindentation for the mechanical characterisation of such layers.

Many research works about the characterisation of the mechanical properties of materials by using the nanoindentation technique have been published in the last years. However, the amount of papers dealing with the use of nanoindentation method to characterise SPS layers is much more scarce [11,12]. Wang et al. [13] have investigated YSZ coatings obtained by APS, from nanostructured powder. The coatings showed a bimodal microstructure made up of molten and partially molten zones meanwhile each of these zones exhibited different hardness and elastic modulus. Lugscheider et al. [14] concluded that the mechanical properties in vertical and horizontal directions are different for TBCs obtained by EB-PVD. Gross and Saber-Samandari [15] studied hydroxyapatite coatings obtained by SPS, concluding that, despite being more porous than those obtained by conventional APS, the overall coating hardness was also similar because the hardness of non-porous areas was also very high. Finally, the authors of this research have recently reported some works on the use of nanoindentation technique for mechanical characterisation of APS and SPS coatings. In a first paper

* Corresponding author at: Instituto de Tecnología Cerámica (ITC). Av. Vicent Sos Baynat s/n, 12006 Castellón, Spain. Tel.: +34 964 34 24 24; fax: +34 964 34 24 25.

E-mail address: emilie.bannier@itc.uji.es (E. Bannier).

Table 1
Operational spray parameters.

Sample	Power (kW)	Ar flow rate (slpm ^a)	H ₂ flow rate (slpm)	Spray distance (mm)	Linear speed (mm/s)	Injection pressure (bar)	Feed suspension flow rate (g/min)	T _{max} (°C)
1	40	40	5	40	250	1.5	13	460
2						3.5	20	420
3					300	2	16	340
4					350	1.5	13	310
5						3.5	20	310

^a slpm: standard litre per minute.

[16], the crystalline phases anatase and rutile were identified in TiO₂ coatings obtained by SPS by nanoindentation technique on the basis of the difference in hardness of these two phases. Similarly, in WC–Co coatings obtained by APS carbide phases with different hardness values were successfully identified [11].

In the present study, a commercial suspension of YSZ nanoparticles was deposited by SPS. In order to address the effect of the spraying parameters, a factorial model was used to design the experiments, meanwhile the effect of both spraying translation speed and injection pressure was considered. Finally, coatings were also microstructurally and mechanically characterised, and the influence of the spraying parameters on microstructure and mechanical properties was evaluated. The mechanical properties were determined using a nanoindenter.

2. Experimental techniques

2.1. Materials

A commercial aqueous suspension of 3 mol% yttria-stabilised zirconia (YSZ) nanoparticles (MELOx Nanosize 3Y, Mel Chemicals, United Kingdom) was used as feedstock. According to the information provided by the supplier, particle specific surface area is 85–96 m²/g and particle average size is 11–12 nm. Fraction of solid in the suspension is approximately 5 vol.%.

TEM observations (H710, Hitachi, Japan) of the nanoparticles in this suspension confirmed their nanometre size (10–20 nm). XRD analysis (D5000, Siemens, Germany) indicated that the powder contains tetragonal phase.

AISI 304 stainless steel specimens in the form of 25 mm diameter and 10 mm thickness discs were used as substrates. Before deposition, the substrates were grit blasted with corundum and cleaned with acetone in an ultrasound bath.

2.2. Coating deposition

All coatings were sprayed using an internal radial injection torch (SG-100, Praxair, USA). This torch was adapted for SPS and a pneumatic system was used to transport the liquid to the injector. This system consists of two pressurised containers so that the liquid inside them is forced to flow to the injector. This device had a 150 µm diameter hole and it was connected to the plasma gun. A filter was used to remove agglomerates larger than 100 µm and probable contaminations. Suspension feeding rate was controlled by adjusting the pressure in the suspension containers. Samples were mounted on a rotating device and up to 6 samples were coated simultaneously.

The main spraying parameters used for each sample, including the reference of the sample, are given in Table 1. In this work, full factorial design of experiments 2^k with a middle point [17] was used in order to study the influence of the parameters on the coating microstructure and properties. In this case, two parameters varied (injection pressure and spraying linear speed) and two levels for each parameter were considered. Moreover, a middle point was established where the parameters were set to the average value of the other two levels. The midpoint was chosen using the experience of previous works [18]. Cooling was performed with compressed air (4 bar). During deposition, the temperature of the samples was measured using a pyrometer (In 5 Plus, Impac, France). Each 3 spraying passes, the deposition was stopped, samples were cooled down to 80 °C, and their thickness was measured using a manual micrometre in order to adjust the number of passes and obtain approximately 70 µm thick coatings.

2.3. Coating characterisation

The microstructure of coating surfaces and cross-sections was characterised by field emission scanning electron microscopy (FEG-SEM, S-4800, Hitachi, Japan). In addition, X-ray diffraction patterns of the coatings were collected using the diffractometer D5000 (Siemens, detector Sol-XDet, CuKα 0.5406 nm, operating at 40 kV–30 mA). Besides, a HORIBA Jobin Yvon Raman spectrometer configured at 514.5 nm

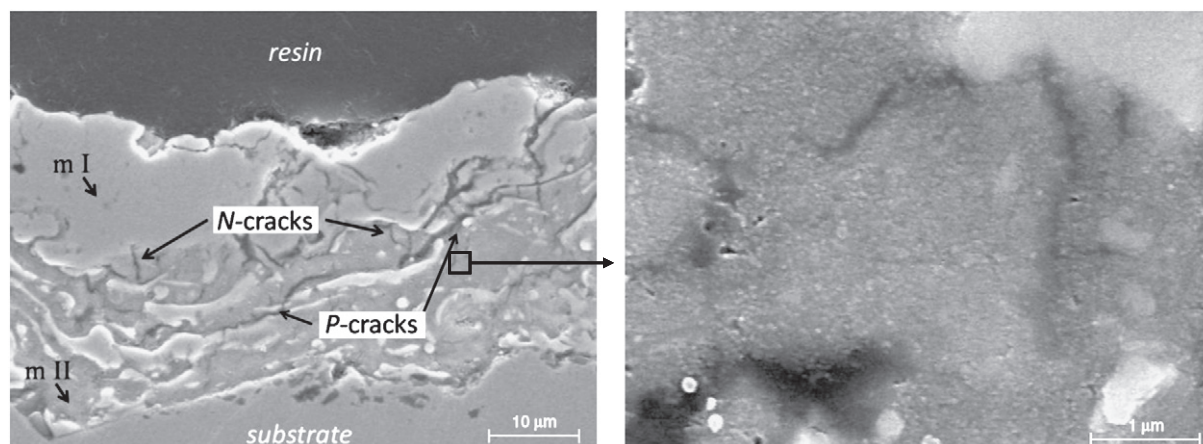


Fig. 1. Cross-sectional FEG-SEM image (secondary electrons) of the as-sprayed YSZ barrier (sample 1) at different magnifications. Low magnification micrograph (left side) shows the bimodal microstructure of molten areas (m-I) and unmolten areas (m-II), the normal cracks (N-cracks) and parallel cracks (P-cracks) with respect to the substrate. High magnification micrograph (right side) shows the fine particles in the unmolten zones.

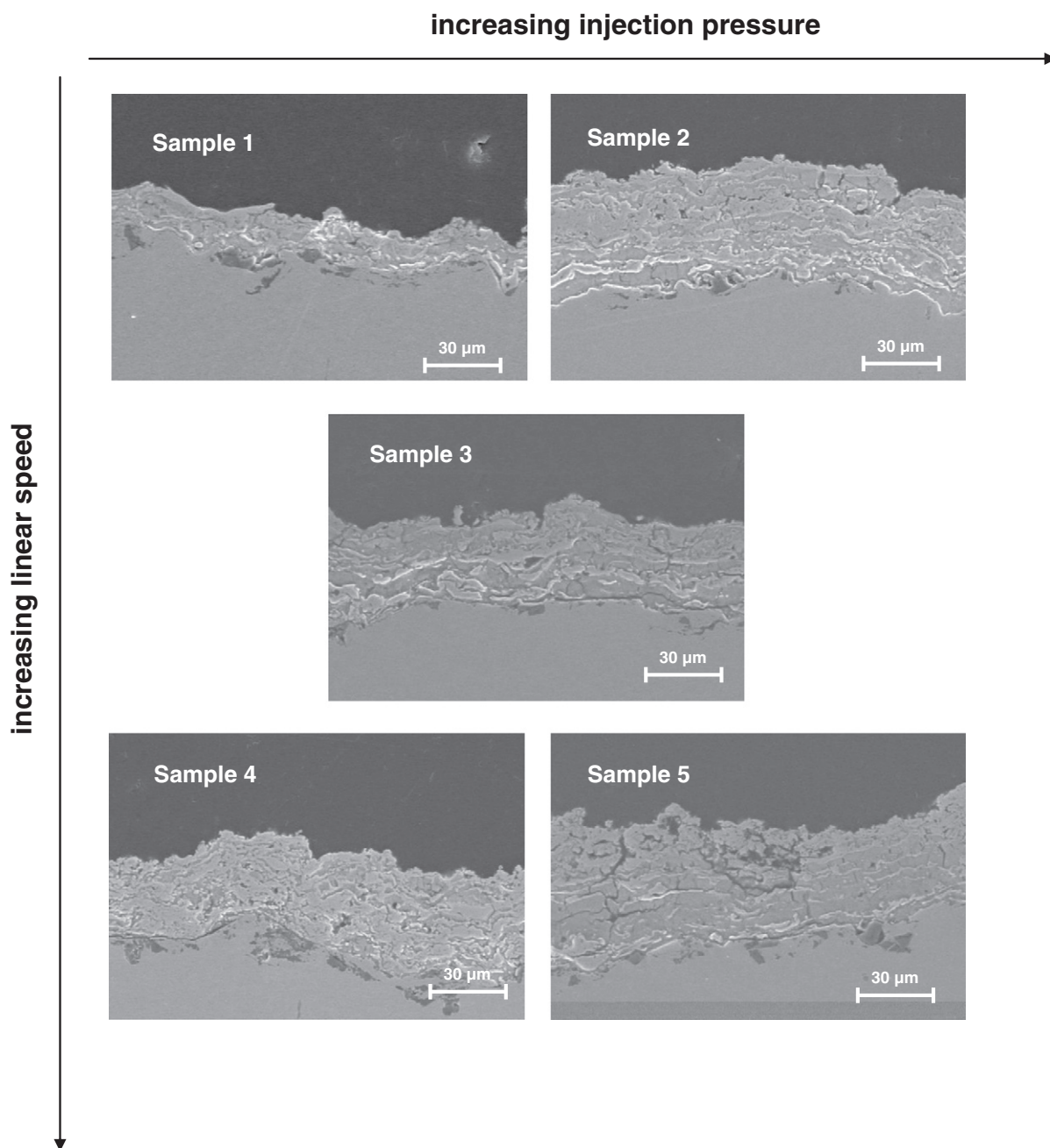


Fig. 2. Cross-section FEG_SEM micrograph (secondary electrons) of the SPS coatings.

emission was used to characterise some of the coated sample cross-sections. The Raman technique used was the microprobe type with spot diameter lower than 1 μm . The localisation of the analysis spot of the argon-ion laser was driven by an optical microscope.

The nanoindentation tests were performed by a G-200 nanoindenter from Agilent Technologies using a previously calibrated diamond Berkovich tip on silica reference material. The stiffness was calculated by a Continuous Stiffness Measurement (CSM) mode set at 2 nm harmonic oscillation amplitude and at 45 Hz oscillation frequency. CSM is a convenient technique for measuring hardness and elastic modulus at small depths. Its main advantage consists in allowing a continuous measurement of basic mechanical properties during loading with the indenter [19]. The location of tests was guided by an optical microscope included in the nanoindenter machine. Indentations were performed on

the polished sample at the cross-sectional view and at a constant 2000 μm depth. Details of this method were previously reported [11,16].

3. Results and discussion

The operational spray parameters influenced considerably the maximum temperature reached by the coatings during the deposition (Table 1). Firstly, when the linear speed increased, the maximum temperature decreased. On the other hand, when the injection pressure increased, the maximum temperature decreased too. The injection pressure is correlated with the suspension feedrate which grows at higher pressure and, consequently, a greater part of the plasma enthalpy is used to evaporate the solvent.

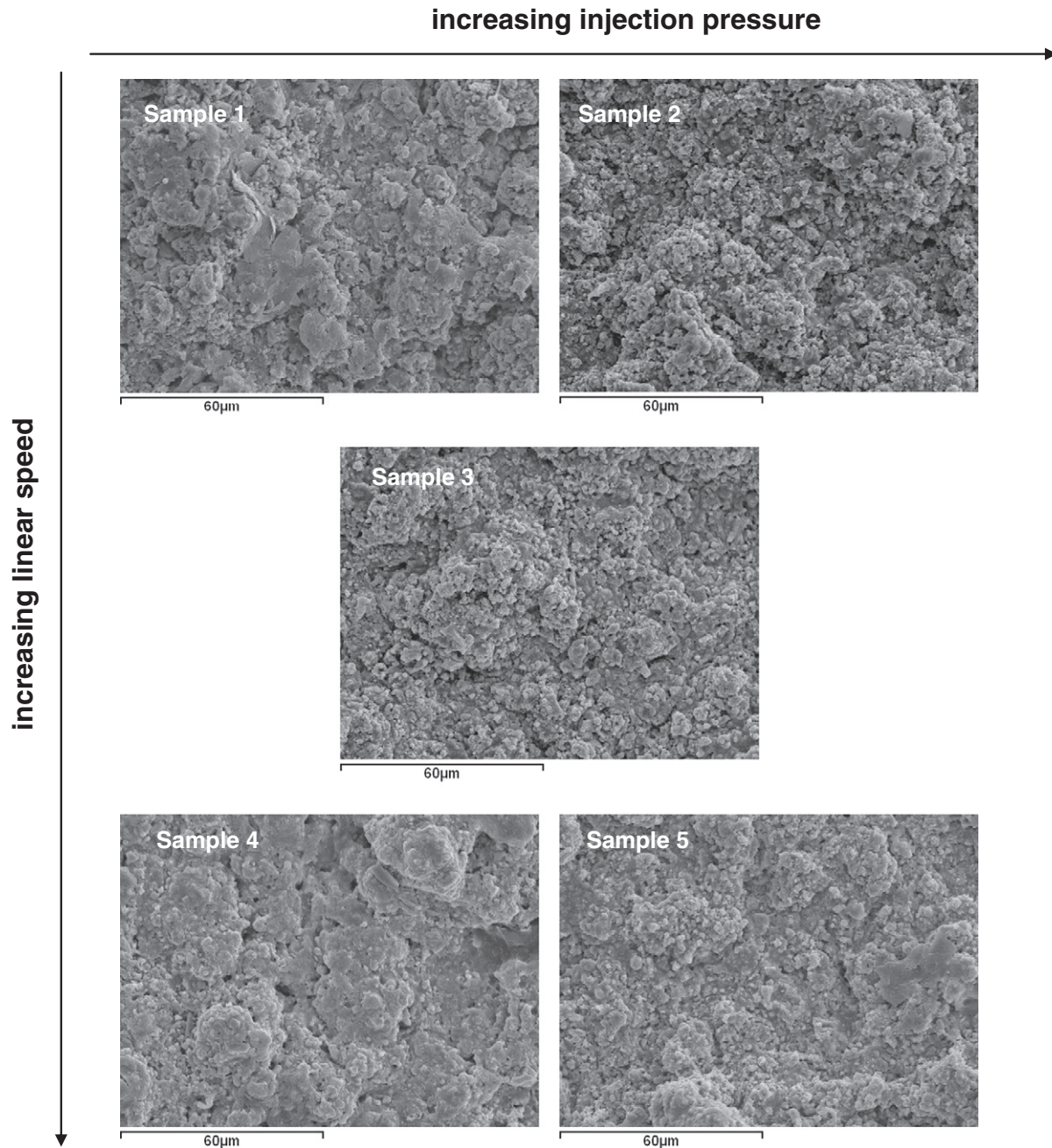


Fig. 3. Surface FEG_SEM micrograph (secondary electrons) of the SPS coatings.

The cross-sectional SEM images of the as-sprayed coatings (sample 1) revealed *two-zone* microstructure, named as (I) molten and (II) sintered grain areas (Fig. 1). The revealed microstructure is caused by different degrees of melting of particles arriving the substrate during the coating growth. Some of the YSZ powder particles were molten and formed the agglomerates during their flight in the jet, while a great quantity of fine powder reached the substrate without being molten as can be seen in the high magnification micrograph shown in Fig. 1. The lamellar microstructure is typical not only for the coatings produced by APS technology but can also be found in the SPS coatings [20]. The lamellas were visible in zones where the molten particles impacted the previously deposited molten particles. Nevertheless, some fine powder was also deposited and sintered during coating growth. This fine particle microstructure contains several cracks growing in the direction normal to the substrate. The cracks are referred later on as *N-cracks*. The *N-cracks* go through the entire

thickness of the unmolten particle microstructure and it looks like that the neighbour molten areas served as crack-barriers. This type of cracks is evidencing stresses generated in the coating probably due to differences of the volumetric expansion of the system substrate-coating and by the temperature gradients occurring during the spraying process. However, several cracks grow parallel to the substrate (*P-cracks*) at the molten grain boundaries, indicating poor cohesion. The *P-cracks* are the most undesired defects because they can induce the delamination failures [21,22].

Among all the obtained coatings, little difference can be found in the cross-section (Fig. 2) and surface (Fig. 3) micrographs. However, sample 1 displayed a much smaller thickness, probably related to a thickness measurement error with the manual micrometre. On the other hand, samples 2, 3 and 4 exhibit fairly homogeneous microstructure when compared with sample 5 (comparison with sample

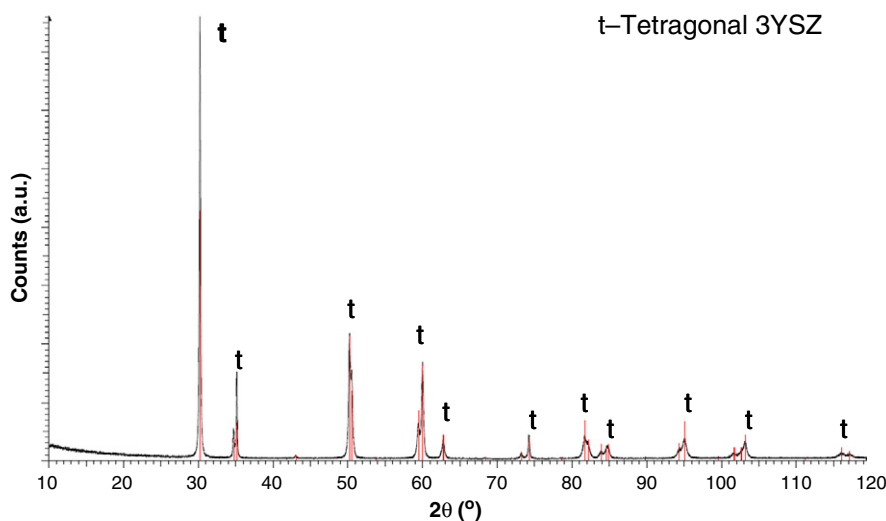


Fig. 4. XRD diagram of sample 3.

1 is difficult owing to its reduced thickness). This homogeneous microstructure comprises fewer and shorter cracks which should result in better coatings mechanical and thermal properties. Nevertheless a relationship between spraying conditions and final microstructure is not evident since samples 2, 3 and 4 were deposited using very different spraying conditions. In fact, these samples belong to the matrix diagonal in the experiment design. On contrary what is clearer in this research is that the combination of a high linear speed and low injection pressure of sample 5 gave rise to a more porous and heterogeneous coating as evidenced by cross-section and top-surface micrographs in Figs. 2 and 3.

The XRD patterns of all coatings show only the presence of tetragonal phase (Fig. 4). This is the usual phase in as-sprayed coatings when the yttria proportion is 3 mol% [23]. Further microprobe Raman analysis confirmed the XRD results set out above, indicating that both zones of

microstructures (unmolten and molten grains) correspond to the same tetragonal phase.

As mentioned above the use of the nanoindentation technique is justified by the limited thickness of the coatings, being difficult to characterise them by means of other standardised microhardness techniques. Although this type of coatings produces an undesirable effective roughness for nanoindentation analysis, the tests were executed carefully on the flat surface reducing the roughness effect. These locations were then chosen on the molten areas (*I*) and on the sintered zones (*II*) of sample 2, as Fig. 5 shows. Furthermore, several indentations were performed on locations with a mixture of both microstructures (*I + II*).

Figs. 6 and 7 show the hardness and elastic modulus obtained for each zone tested, respectively. Below 1 μm depth the great dispersion of values is justified by the roughness and by the heterogeneity of

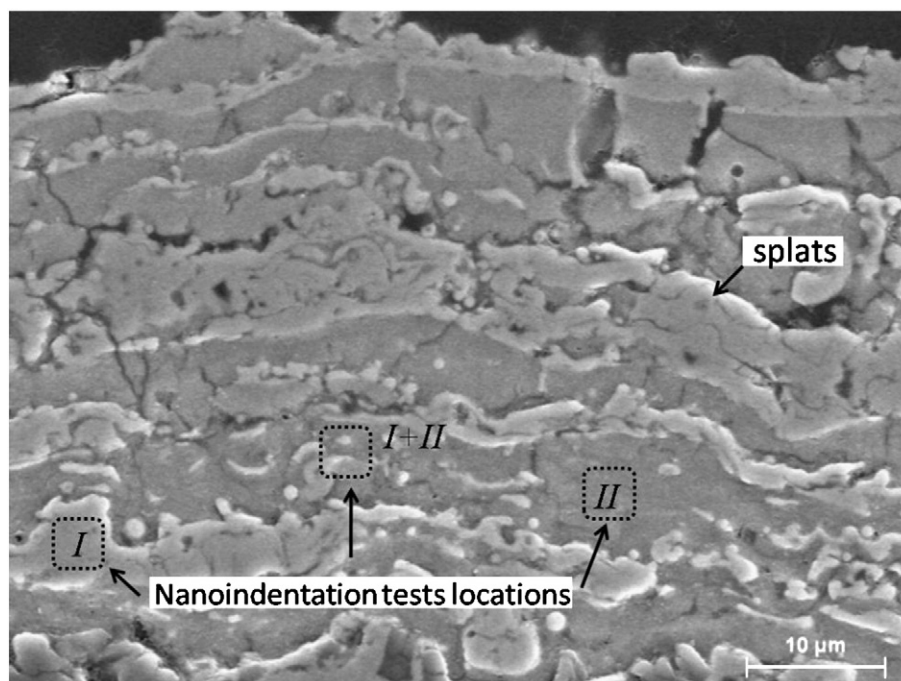


Fig. 5. FEG-SEM micrograph (secondary electrons) of the cross-section of the as-sprayed YSZ coatings (sample 2). The nanoindentation test was performed on molten areas (*m-I*) and fine particle microstructure (*m-II*) in order to test flat surfaces.

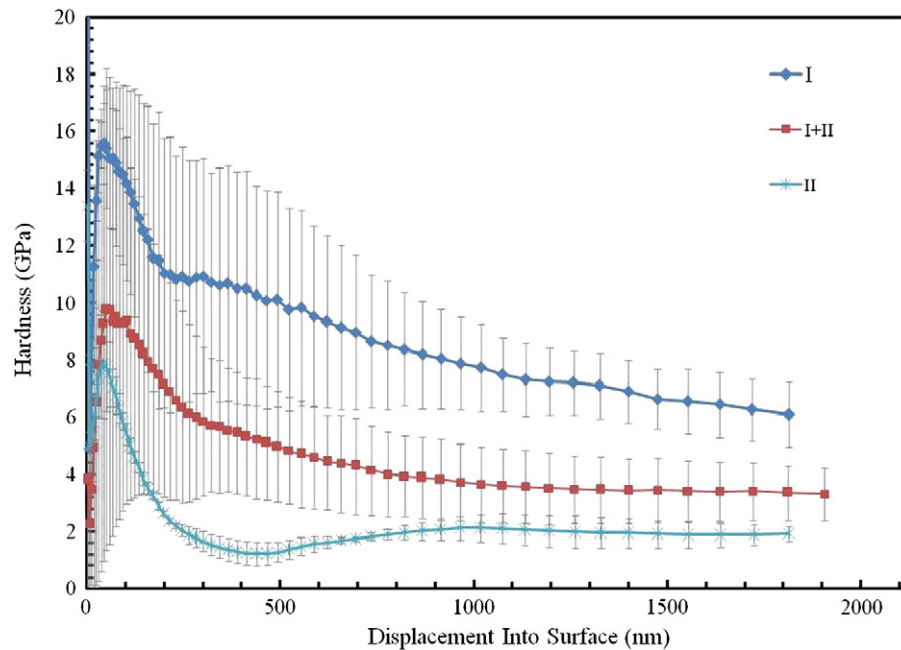


Fig. 6. Nanoindentation hardness curves for the analysed microstructures shown in Fig. 5 (sample 2).

microstructure beyond the indenter. Even so, three tendencies were clearly observed in depth for H and E curves. Hardness results acquired for the molten grains zone (I) at the experimented load interval ranged from 8 GPa to 12 GPa, while hardness in the matrix of sintered grains (II) was stabilised at 2 GPa. The indentations which achieved mixture of microstructures showed hardness values stabilised at 4 GPa as expected by the mixture law. The E and H values agreed with the reported tendency in nanostructured APS YSZ coatings [13] and nanostructured YSZ coatings obtained by SPS [12]. With regard to elastic modulus findings, the obtained values ranged from 125 to 150 GPa for molten areas and 65 GPa for the matrix. Recently, Łatka et al. have successfully identified by nanoindentation technique, the *two-zone* microstructure in suspension plasma sprayed hydroxyapatite coatings. These authors found that the different hardness of dense and sintered zone gave rise

to two general types of indentation curves [24]. However, Wang et al. [13] showed that nanostructured YSZ coatings obtained by APS also exhibited a bimodal distribution of mechanical properties (H and E), which corresponded to the molten and partially molten zones. In addition, an estimate of the elastic modulus on the basis of the two different microstructures (unmolten and molten zones) forming the coating layer was successfully determined. However, no paper was found that reports a bimodal distribution of nanoindentation mechanical properties (H and E) in YSZ coatings obtained by SPS.

The reason of the strong differences observed in both hardness and elastic modulus, in the different zones forming the coatings addressed in the present work is basically due to the characteristic microstructure of these zones, as can be also seen in other studies. The relationship of mechanical properties with microstructure in

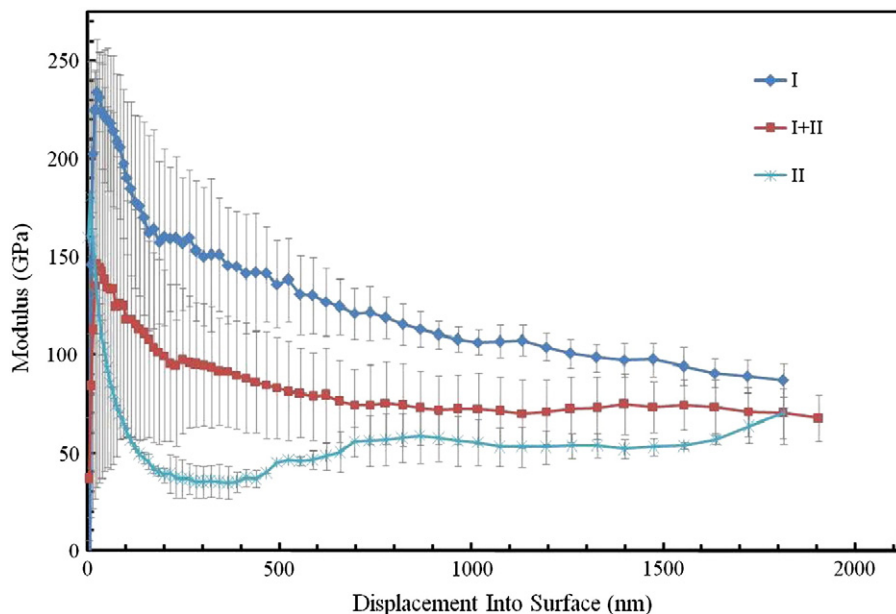


Fig. 7. Nanoindentation Young's modulus curves for the analysed microstructures shown in Fig. 5 (sample 2).

TBCs obtained by APS has been reported elsewhere by means of other characterisation techniques. Steinbrech et al. [25,26] showed that TBC mechanical properties, in particular coating stiffness, depended on the deformed volume as well as the applied load as a consequence of the microstructural features of the coatings. These authors reported a strong strain dependency of coating stiffness associated with the number of cracks and pores. In the present work, Fig. 5 displays unmolten or partially molten zones that are made up of partially sintered nanoparticles giving rise to poor interparticle bonding. The sintering of the fine grains deposited on the substrate was previously proved to occur in the experimental conditions of different suspension plasma sprayed coatings [27]. On contrary, molten particles lead to stronger cohesion in the arrangement of nanoparticles improving the mechanical properties. In this sense, mechanical properties such as H and specially E , evaluated by nanoindentation can be considered a good fingerprint of the type of microstructure developed in the deposit during the SPS process.

4. Conclusions

YSZ suspension was successfully deposited by SPS. A 2^k experiment with a middle point design was used in order to search the influence of operational spray parameters onto coating microstructure and mechanical properties. All coatings displayed a *two-zone* microstructure with fully molten areas and sintered-grains areas where the nanostructure is exhibited.

The coating obtained using middle point parameters presented the most homogeneous microstructure. The nanoindenter showed two well-distinguished zones throughout the coatings, which displayed different hardness and elastic modulus. Molten zones exhibit higher values of hardness and elastic modulus than those of the sintered-grain zone. In addition, the mechanical properties of the overall coating could be estimated from the average value between the mechanical properties of the two zones. Thus, nanoindentation has been proved to be a powerful tool to achieve a suitable mechanical characterisation of the thin layers obtained in SPS coatings.

Acknowledgements

This work has been supported by the Spanish Ministry of Science and Innovation (project MAT2009-14144-C03) and the Research Promotion

Plan of the Universitat Jaume I, action 2.1 (ref. E-2011-05) and action 3.1 (ref. PREDOC/2009/10). The authors are grateful to Leszek Łatka for his help in plasma spray experiments.

References

- [1] L. Lima, B.R. Marple, J. Therm. Spray Technol. 16 (1) (2007) 40.
- [2] D. Chen, E.H. Jordan, M. Gell, J. Therm. Spray Technol. 18 (3) (2009) 421.
- [3] R.S. Lima, B.R. Marple, Mater. Sci. Eng., A 485 (1–2) (2008) 182.
- [4] P. Fauchais, G. Montavon, R.S. Lima, B.R. Marple, J. Phys. D: Appl. Phys. 44 (9) (2011) 093001.
- [5] A. Killinger, R. Gadow, G. Mauer, A. Guignard, R. Vassen, D. Stöver, J. Therm. Spray Technol. 20 (4) (2011) 677.
- [6] A. Bacciochini, G. Montavon, J. Ilavsky, A. Denoirjean, P. Fauchais, J. Therm. Spray Technol. 19 (1–2) (2010) 198.
- [7] H. Kassner, R. Siegert, D. Hathiramani, R. Vassen, D. Stoeve, J. Therm. Spray Technol. 17 (1) (2008) 115.
- [8] L. Łatka, A. Cattini, L. Pawłowski, S. Valette, B. Pateyron, J.-P. Lecompte, R. Kumar, A. Denoirjean, Surf. Coat. Technol. 208 (2012) 87.
- [9] K. VanEvery, M.J.M. Krane, R.W. Trice, H. Wang, W. Porter, M. Besser, D. Sordet, J. Ilavsky, J. Almer, J. Therm. Spray Technol. 20 (4) (2011) 817.
- [10] E. Meillot, R. Vert, C. Caruyer, D. Damiani, M. Vardelle, J. Phys. D: Appl. Phys. 44 (2011) 194008.
- [11] E. Rayón, V. Bonache, M.D. Salvador, J.J. Roa, E. Sánchez, Surf. Coat. Technol. 205 (17–18) (2011) 4192.
- [12] R. Vert, D. Chicot, C. Dublanche-Tixier, E. Meillot, A. Vardelle, G. Mariaux, Surf. Coat. Technol. 205 (4) (2010) 999.
- [13] L. Wang, Y. Wang, X.G. Sun, J.Q. He, Z.Y. Pan, C.H. Wang, Vacuum 86 (8) (2012) 1174.
- [14] E. Lugscheider, K. Bozkin, S. Barwulf, A. Etzkorn, Surf. Coat. Technol. 138 (1) (2001) 9.
- [15] K. Gross, S. Saber-Samandari, Surf. Coat. Technol. 203 (20–21) (2009) 2995.
- [16] E. Rayón, V. Bonache, M.D. Salvador, E. Bannier, E. Sánchez, A. Denoirjean, H. Ageorges, Surf. Coat. Technol. 206 (10) (2012) 2655.
- [17] C. Pierlot, L. Pawłowski, M. Bigan, P. Chagnon, Surf. Coat. Technol. 202 (18) (2008) 4483.
- [18] S. Kozerski, L. Łatka, L. Pawłowski, F. Cernuschi, F. Petit, C. Pierlot, H. Podlesak, J.P. Laval, J. Eur. Ceram. Soc. 31 (12) (2011) 2089.
- [19] G.M. Pharr, J.H. Strader, W.C. Oliver, J. Mater. Res. 24 (3) (2009) 653.
- [20] S. Kozerski, L. Pawłowski, R. Jaworski, F. Roudet, F. Petit, Surf. Coat. Technol. 204 (9–10) (2010) 1380.
- [21] G. Di Girolamo, F. Marra, C. Blasi, E. Serra, T. Valente, Ceram. Int. 37 (7) (2011) 2711.
- [22] M. Karger, R. Vaßen, D. Stöver, Surf. Coat. Technol. 206 (1) (2011) 16.
- [23] G. Witz, V. Shklower, W. Steurer, J. Am. Ceram. Soc. 91 (8) (2007) 1.
- [24] L. Łatka, L. Pawłowski, D. Chicot, C. Pierlot, F. Petit, Surf. Coat. Technol. 205 (4) (2010) 954.
- [25] T. Wakui, J. Malzbender, R.W. Steinbrech, Surf. Coat. Technol. 200 (16–17) (2006) 4995.
- [26] J. Malzbender, R.W. Steinbrech, J. Mater. Res. 18 (8) (2003) 1975.
- [27] L. Łatka, S.B. Goryachev, S. Kozerski, L. Pawłowski, Mater. 3 (2010) 3845.